RSC Advances

PAPER

View Article Online
View Journal | View Issue

Cite this: *RSC Adv.*, 2021, **11**, 24536

Hydrothermal green synthesis of MoS_2 nanosheets for pollution abatement and antifungal applications†

Mengistu Mulu,[a] Dharmasoth RamaDevi,[b] Neway Belachew *[c] and K. Basavaiah *[a]

Received 16th May 2021
Accepted 8th July 2021

DOI: 10.1039/d1ra03815j

rsc.li/rsc-advances

In this study, we report a green synthesis of MoS_2 nanosheets (NSs) using a facile hydrothermal technique in the presence of L-cysteine. L-Cysteine can serve as a greener source of sulfur as well as a capping agent to help the growth of MoS_2 nanosheets. The prepared materials were characterized by X-ray powder diffraction (XRD), scanning electron microscopy (SEM) with energy dispersive spectroscopy (EDS), electron transmission microscopy (TEM), X-ray photoelectron microscopy (XPS), and Brunauer, Emmett, and Teller (BET) analysis. The results showed that MoS_2 NSs are of high crystallinity with a lattice spacing of 0.61 nm. The optical bandgap of MoS_2 NSs nanosheets prepared using L-cysteine as a source of sulfur was found to be 1.79 eV. The photocatalytic degradation of MoS_2 NSs towards methylene orange (MO) and rhodamine blue (RB) dyes under sunlight was found to be promising for practical applications. The fast kinetics of degradation of MO and RhB was observed over a wide range of pH range. Moreover, MoS_2 NSs showed excellent antifungal activities against *Trichophyton mentagrophytes* and *Penicillium chrysogenum* fungus.

1. Introduction

During the last decades, the rapid increase in industrialization and human population has brought a multitude of contaminants to the aquatic environment. Synthetic organic dyes from dyeing industries make a substantial contribution.[1] Due to this millions of people have been dying every year because of water pollution.[2] Therefore, it is a prime concern to reduce or remove pollutants from their point source before releasing them into the environment. Adsorption, Fenton-oxidation, flocculation, and photocatalysis techniques have been widely used to abate toxic effluents.[3–5] Photocatalytic degradation due to their efficiency can degrade pollutants without leaving unwanted residues.[6] TiO_2 and ZnO in this regard play a significant role in the harvesting of light for the photocatalytic degradation of organic compounds.[7] However, inefficient utilization of light in the visible region and high electron–hole recombination rate prohibit its practical applications. Searching or modification of photocatalysts that working efficiently in the visible region is the prime concern in this topic.[8] Composite with different sensitizers, doping of different elements and morphology optimization are common strategies for the modification of photocatalysts.[9] More recently, the combination of photocatalyst with persistent luminescent materials as inner secondary light sources is introduced to enhance the photocatalytic efficiency of semiconductors.[10–12]

Two-dimensional (2D) functional nanostructured materials, such as graphene, hexagonal boron nitride (hBN), graphitic carbon nitride (g-C_3N_4) and metal dichalcogenides (MX_2), owing to their inherent physicochemical properties, including high specific surface-to-volume ratio, anisotropy, chemical inertness, better charge carrier separation, the rich option of host–guest species, and excellent tribological efficiency, have gotten a lot of attention for photocatalytic applications.[13,14] Moreover, they are widely used in a variety of fields, such as lubricants, energy storage, electrocatalysis, magnetoresistance, organic catalysis, sensing, and field transit.[14,15]

Recently, MX_2-based transition metal chalcogenides (TMDs) where M (= Mo, W, *etc.*) is a transition metal of group VI and X (= S, Se, *etc.*) is a chalcogen that has been received a lot of attention owing to unique electrical, optical and mechanical properties. Among 2D nanomaterials, MoS_2 due to intriguing physicochemical properties shows an application in antibacterial,[16,17] biomedical,[18,19] transistors,[20] photodetectors,[21] and, solar cells.[22] Bulk MoS_2 is an indirect bandgap semiconductor. However, as the number of layers is reduced to a few, bilayers, and even monolayers, the bandgap becomes direct.[23] Such

[a]*Department of Inorganic and Analytical Chemistry, Andhra University, Visakhapatnam-530003, India*

[b]*A.U. College of Pharmaceutical Sciences, Andhra University, Visakhapatnam-530003, India*

[c]*Department of Chemistry, Debre Birhan University, Debre Berhan, Ethiopia. E-mail: neway.du@gmail.com; neway@dbu.edu.et*

† Electronic supplementary information (ESI) available: Details of antifungal procedure, BET plot and photographic images of MoS_2 powder. See DOI: 10.1039/d1ra03815j

direct bandgap semiconductor materials are suitable for harvesting light. Hence, the synthesis of MoS_2 with a few layered structures is a prime concern for nanosheets for photocatalytic applications such as dye degradation and solar energy conversion.[24,25]

MoS_2 NSs with enhanced properties have been synthesised by various techniques, including chemical vapour deposition (CVD),[26] thermal reductions,[27] hydrothermal,[28] laser ablation,[29] Liquid Phase Exfoliation (LPE),[30,31] and sol–gel methods.[32,33] Despite the quality of MoS_2 NSs synthesized by the aforementioned techniques, but they require highly sophisticated equipment and commonly used environmental malignant reagents. Most of the synthesis methods were used organic solvents, and surfactants during the synthesis of MoS_2 NSs, which introduce toxicity to the environment and human health. Therefore, searching for kind reagents for the preparation of MoS_2 NSs should require considerable attention. Biomolecule-assisted synthetic pathways have been a promising technique in recent years because they are greener and having suitable chemistry for the preparation of nanomaterials.

Green synthesised nanostructured materials play a significant role in practical applications, including medicinal and environmental. Biological ways of synthesizing nanoparticles using microorganisms, enzymes, fungi, and plants or plant extracts are eco-friendly green synthesis alternatives to chemical and physical methods.[18,19,34–36] In this regard, amino acids due to interesting aqueous chemistry are widely applicable as a reducing agent, capping agent and a source of dopant atoms during the synthesis of nanomaterials.[37] Among these, L-cysteine is a sulphur-containing derivative resulting from the oxidation of the side chains of cysteine amino acid thiol. It functions as an antioxidant, shielding tissues from radiation and toxins and thereby slowing the ageing process. L-Cysteine also reported as a sulphur source for the preparation of MoS_2. For example, 1D CNTs–MoS_2 hybrid materials synthesised by hydrothermal method using L-cysteine as sulphur soured for anodized materials in lithium-ion batteries.[38] Similarly, Veeramalai *et al.*[39] reported MoS_2 layered structure by the reduction of MoO_3 using L-cysteine as a sulphur source. The synthesised MoS_2 showed high field performance applications. Despite the potential of L-cysteine as a source of sulphur and capping agent to protect an irreversible agglomeration, there is no comprehensive report on the facile hydrothermal synthesis and photocatalytic investigation towards dye degradation of MoS_2 NSs.

Hence, we aimed to synthesis MoS_2 NSs using a facile hydrothermal method. $(NH_4)_6Mo_7O_{24}\cdot 4H_2O$ salt and L-cysteine are the only precursors for the preparation of MoS_2 NSs. The electronic, crystal phase formation, composition and surface morphology of the synthesised MoS_2 nanosheet powder was investigated by UV-Vis, UV-DRS, XRD, FT-IR, XPS, TEM/SAED, and FE-SEM/EDX. The Brunauer–Emmett–Teller (BET) method used to determine the surface area analysis. The photocatalytic activities MoS_2 NSs was investigated by the degradation of the two stable organic dyes, such as rhodamine B (RhB) and methylene orange. These two dyes commonly found in industrial wastewater and are extremely toxic to human health due to their solubility, carcinogenicity, and teratogenicity. Moreover, the antifungal activity of MoS_2 was studied against *Penicillium chrysogenum* and *Trichophyton mentagrophytes* fungus.

2. Experimental

2.1. Materials

All of the chemicals used in this analysis were analytical grade levels from Sigma-Aldrich, and Himedia. All chemicals were directly used without further purification. Specifically, ammonium molybdate tetrahydrate $[(NH_4)_6Mo_7O_{24}\cdot 4H_2O]$, and L-cysteine ($C_3H_7NO_2S$) were obtained from Himedia, India. Methylene orange (MO), and rhodamine blue (RhB) were supplied from Sigma-Aldrich, India. The ultrapure water (Milli-Q) was used as a solvent throughout the whole experiment.

2.2. Nanosheet MoS_2 synthesis

MoS_2 NSs were synthesized by a facile and green hydrothermal synthesis approach using L-cysteine as a sulphur source. Particularly, 2.0 g $(NH_4)_6Mo_7O_{24}\cdot 4H_2O$ and 4.0 g L-cysteine were mixed in 50 mL deionized water. The solution was then sonicated for 30 minutes to create a clear solution. In a muffle furnace, the solution was poured into a 100 mL stainless steel autoclave and heated at 200 °C for 12 hours (Fig. 1). The autoclave was cooled to room temperature after the reaction had completed. Next, the black precipitate was centrifuged and thoroughly washed with water to remove unreacted residue and dried in the oven at 70 °C for 18 hours. The black powder, the as-synthesised MoS_2 nanosheet, was kept for further use (ESI, Fig. 1†).

2.3. Characterizations

PANalytical Xpert Pro diffractometer with, Cu $K_1 = 0.154056$ nm as a radiation source was used to record the X-ray diffraction (XRD) of MoS_2 NSs. Transmission electron microscopy (TEM) images were recorded from FEI TECNAI G2 S-Twin, equipped with a 200 kV field emission gun (FEG). The field emission scanning electron microscopy (FE-SEM) images were obtained from JEOL, JSM-7600F SEM at an accelerated voltage of 0.1 to 30 kV equipped with X-ray dispersive spectroscopy (EDX). The chemical composition of the MoS_2 NSs was detected by X-ray

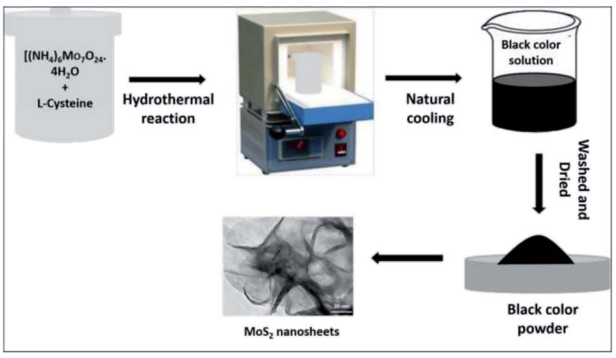

Fig. 1 The schematic illustration for the hydrothermal synthesis of MoS_2 NSs.

photoelectron spectroscopy (XPS, ESCALAB 250Xi). The Brunauer–Emmett–Teller (BET) (BELSORB-28SA/18SA/18PLUS) analyser studied the surface area and pore size from the N_2 adsorption data.[40,41]

2.4. RhB and MO photocatalytic degradation

The photocatalytic activity of the MoS_2 NSs towards the degradation of MO and RhB was investigated under natural sunlight irradiation. The adsorption–desorption equilibrium of dye was carried in the dark for 30 min before illumination. Specifically, 30 mg of MoS_2 NSs was taken for 50 mL of 20 ppm dye solution. The sample was in dark to attain the adsorption–desorption and illuminate at midday (11 am to 3 pm) sunlight. At different time intervals, 3 mL of the solution took from the reaction vessel and centrifuged at 5000 rpm for 5 min to separate the catalyst. The residual concentration of MO and RhB in the solution was determined using a UV-visible spectrophotometer at λ_{max} = 500 nm and 553 nm, respectively. The quantitative explanation of adsorption in the dark and degradation under sunlight was calculated by eqn (1) and (2) respectively.

$$q = (C_0 - C_t) \times V/m \quad (1)$$

$$\text{Degradation (\%)} = (C_0 - C_t) \times 100/C_0 = \quad (2)$$

where q (mg g^{-1}) the amount of MO adsorbed on the surface of MoS_2 nanosheet; V (L) is the volume of the aqueous solution, m (g) is the mass of MoS_2 nanosheet, C_0 (mg L^{-1}), the initial concentration of MO/RhB dye; C_t (mg L^{-1}) the concentration of MO/RhB dye after adsorption/degradation. Furthermore, the antifungal activities of MoS_2 NSs using Agar-Well diffusion method was further investigated against the *T. mentagrophytes* and *P. chrysogenum* fungus. The detailed protocol presents in ESI 1.†

3. Results and discussion

3.1. Characterizations of MoS_2 nanosheets

The UV-Vis absorption spectrum of MoS_2 NS was recorded to investigate the optical property. As shown in Fig. 2, the absorption edge of MoS_2 NS extends to the visible region.

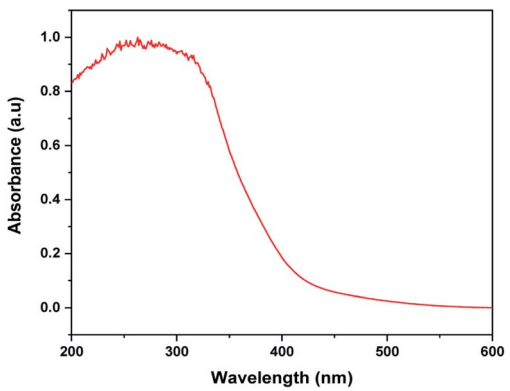

Fig. 2 The UV-Vis absorption spectrum of MoS_2 NSs.

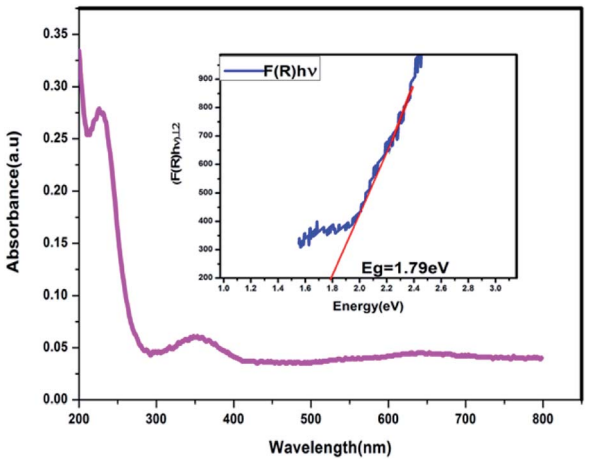

Fig. 3 The UV-DRS absorption spectrum of MoS_2 NSs.

Moreover, the optical bandgap energy of MoS_2 NS was calculated from the UV-DRS spectrum (Fig. 3). The intrinsic direct bandgap of MoS_2 NSs was found to 1.79 eV. This implies that the activation [formation of electron (e^-) and holes (h^+)] of MoS_2 NSs is possible under the irradiation of the visible light region. Similar bandgap energy reported elsewhere.[34]

Fig. 4 shows the XRD pattern for MoS_2 NSs. The diffractogram confirms the formation of hexagonal MoS_2 NSs from Mo^{2+} salt and L-cysteine as a sulfur source. The characteristic diffraction peak observed at 13.6°, 31.97°, 32.39°, 36.53°, 40.26°, 42.39°, and 48.94° which are indexed to (002), (100), (101), (102), (103), (106), and (105) planes of MoS_2, respectively (JCPDS#: 00-037-1492).[42] The broadened of the (002) peak and diffraction at a low angle (2θ: 13.6°) than bulk MoS_2 (14.37°) shows the formation of few or single layers of MoS_2 like graphene.[43]

The FTIR spectrum of the MoS_2 NSs was recorded to investigate the composition of samples based on the vibrational properties (Fig. 5). The spectrum of MoS_2 NSs shows the broad bands between 3748 and 3400 cm^{-1} attribute to the characteristics of O–H stretching of the intermolecular and intramolecular hydrogen bonds.[44,45] The characteristic vibrational

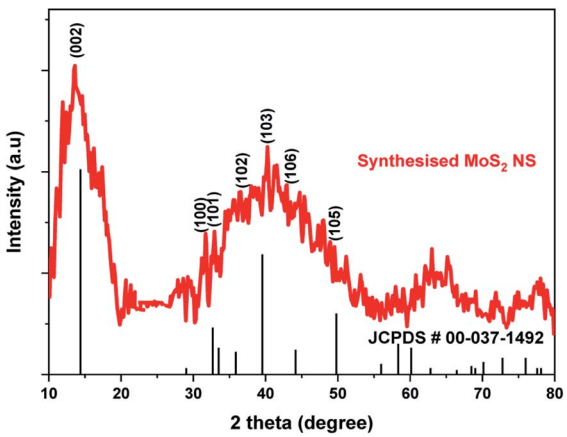

Fig. 4 The XRD graph of MoS_2 NSs.

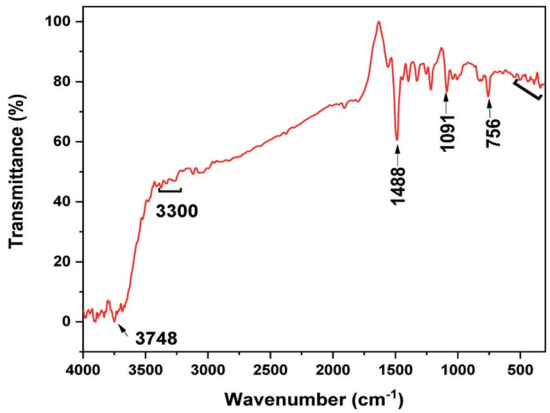

Fig. 5 The FT-IR spectrum of MoS_2 NSs.

bands at 3300–2800 cm^{-1} and 1488 cm^{-1} can be assigned to the stretching of the C–H alkyl stretching band in L-cysteine.[46] Thus, the FTIR results further affirmed the presence of residual amino acid on the surface of MoS_2. The medium absorption bands observed at 756 cm^{-1}, 1091 cm^{-1}, and 1400 cm^{-1} are due to MoS_2.[47,48] Moreover, the band between 540 cm^{-1} and 400 cm^{-1} credit to the S–S bond vibrations.[47]

The composition and chemical state of MoS_2 NSs was studied by X-ray photoelectron spectroscopy (XPS). Fig. 6a presents the survey scan XPS spectrum of MoS_2 NS. The spectrum depicts the presence of peaks due to C_{1s} and O_{1s} at 285.49 eV and 533.07 eV respectively. These are due to the residual L-cysteine capped onto the MoS_2 surface. The high-resolution peaks of Mo, S, and O are shown in Fig. 6b–d. The peak binding energies of Mo and S are agreed well with the theoretical binding energies of the corresponding orbital electrons of Mo and S elements. Further, both the Mo $3d_{5/2}$ (227.48 eV) and the Mo $3d_{3/2}$ (230.63 eV) features presented in Fig. 6b are deconvoluted with only one function, indicating the presence of only one molybdenum chemical species at the surface.[49,50] Moreover, the binding energy shows a shift as compared to the elemental Mo peaks affirms the formation of

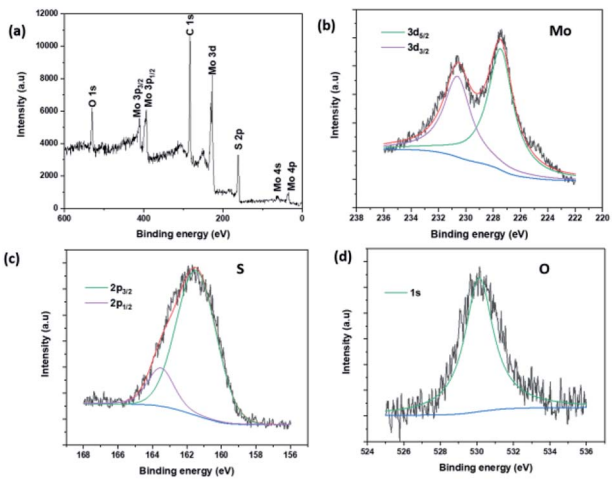

Fig. 6 (a) The survey XPS spectrum of MoS_2 NSs, (b–d) the high-resolution XPS spectra of Mo, S and O, respectively.

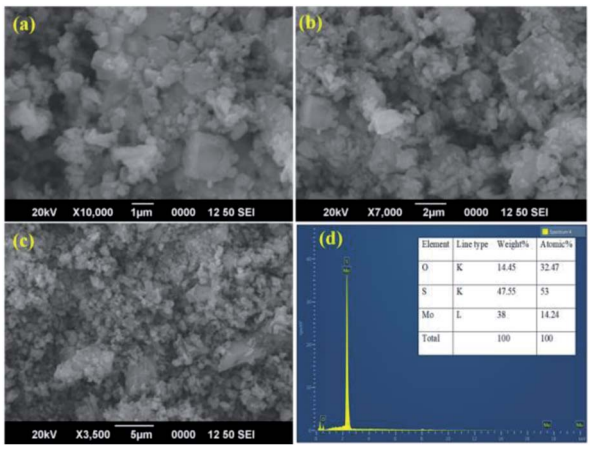

Fig. 7 (a–c) The representative SEM images NSs at different magnifications, (d) EDS spectrum of MoS_2.

Mo^{4+} chemical state.[39,51] Likewise, a similar analysis was done on sulfur, obtained characteristic peaks at the binding energy of 161.58 eV and 162.78 eV due to the S $2p_{3/2}$, and assigned to S $2p_{1/2}$, respectively.[52,53]

SEM and TEM microscopic techniques were used to investigate the surface morphology of MoS_2 NSs. Fig. 7a–c shows the SEM image of the synthesized MoS_2 NSs. The image shows an aggregated and rough surface morphology of MoS_2 NSs. Interesting sheet-like morphology observed under TEM analysis (Fig. 8). As it is shown in Fig. 8a and b, a few layers and aggregated MoS_2 were synthesized *via* a facile hydrothermal method. The selected area electron diffraction (SAED) pattern (Fig. 8c) of the MoS_2 sheet shows the smoothness of the concentric circle, which indicates the poor crystallinity of the sheet. Moreover, the (002), (100), and (001) planes keep stable, indicating the good stability of MoS_2 along this plane.

3.2. RhB and MO dye degradation *via* photocatalysis

The pH of the solution an important factor that affects the surface charge of the photocatalyst and the charge of the

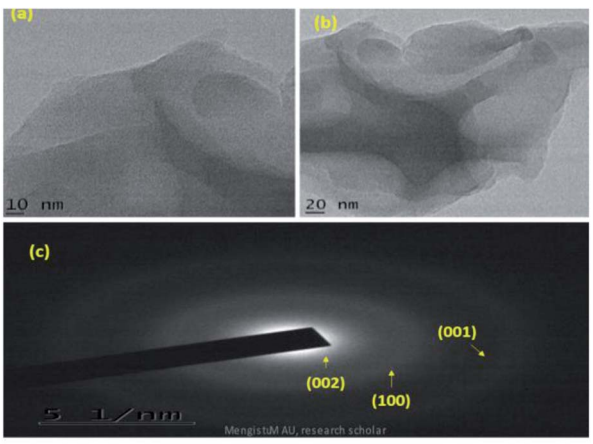

Fig. 8 (a and b) The representative TEM images NSs at different magnifications, (c) SAED pattern of MoS_2.

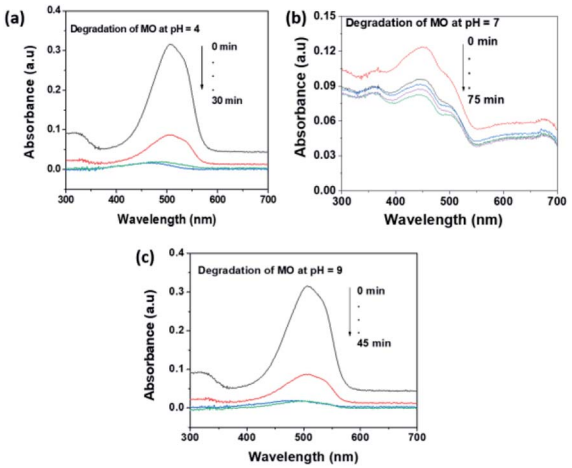

Fig. 9 The effect of pH of solution for the degradation MO at (a) pH = 4, (b) pH = 7 and (c) pH = 9.

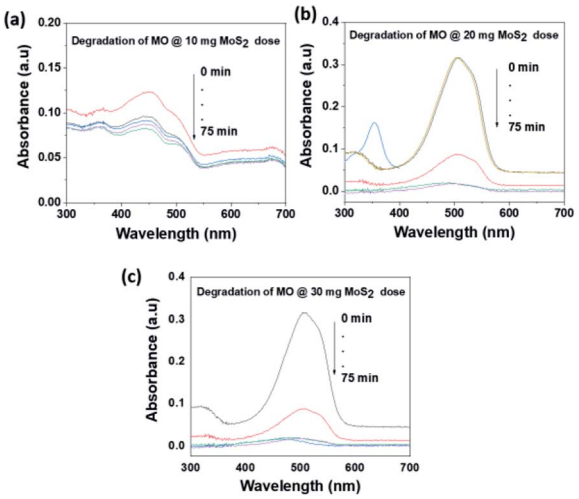

Fig. 11 The effect of MoS_2 NSs dose for the degradation MO.

organic dye. As a result, the electrostatic interaction between the dye molecule and catalyst surface is highly affected by the pH of the solution. Methyl orange (MO) and rhodamine B (RhB) dyes were selected as representative anionic and cationic dyes respectively, for the photocatalytic investigation of MoS_2 NSs. The acidic (pH = 4), neutral (pH = 7) and basic (pH = 9) medium were optimized to study the pH effect. Fig. 9 shows the effect of pH on the photocatalytic degradation of MO. As can be seen in Fig. 9, MoS_2 NSs (30 mg) show a strong potential to degrade MO (20 mg L^{-1}) at a given pH of the solution. Still, degradation of MO shows fast kinetics and almost complete degradations at pH = 4 due to the protonated surface at low pH enhance the electrostatic interaction with the anionic dye. Alkaline pH (pH = 9) also suitable to get a complete degradation of MO slightly at a longer time (Fig. 9c) than acidic. The increase in hydroxyl ions concentration in the solution facilitated the formation of further hydroxyl radical; this could be plausible for an enhanced reaction rate of degradation under alkaline conditions. The neutral pH (pH = 7) shows a relatively poor rate of degradation and efficiency (72%) (Fig. 9b). Hence, the acid or alkaline medium is suggested to get a better photocatalytic degradation efficiency of MO.

A similar investigation on the degradation of RhB performed at various pH of the solution. The potential of MoS_2 NSs also observes for the degradation of a stable RhB dye. As shown in Fig. 10, complete degradation of 50 mL RhB (20 mg L^{-1}) using 80 mg MoS_2 NSs at acid and neutral solutions. Similar justification on the effect of pH for the degradation of RhB is applied to as MO. RhB was successfully removed with a high rate of degradation was observed at neutral pH (Fig. 10b). Concomitantly, the absorption maxima of RhB at $\lambda_{max} = 553$ nm showed a shift to a lower wavelength region during the degradation process, which attributes to the formation of intermediate products in the meanwhile.

The photocatalytic activity of MoS_2 NSs was further investigated at various doses of the catalyst. At a fixed amount of dye concentration (50 mL, 20 mg L^{-1}), at neutral pH and room temperature. Fig. 11 shows the effect catalyst dose for the removal of MO at the various dose of MoS_2 (10 mg, 20 mg, and

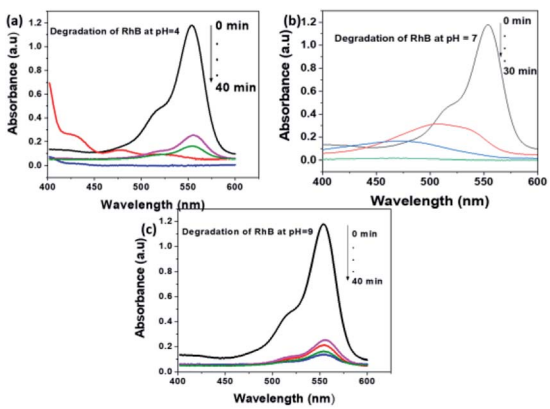

Fig. 10 The effect of pH of solution for the degradation RhB at (a) pH = 4, (b) pH = 7 and (c) pH = 9.

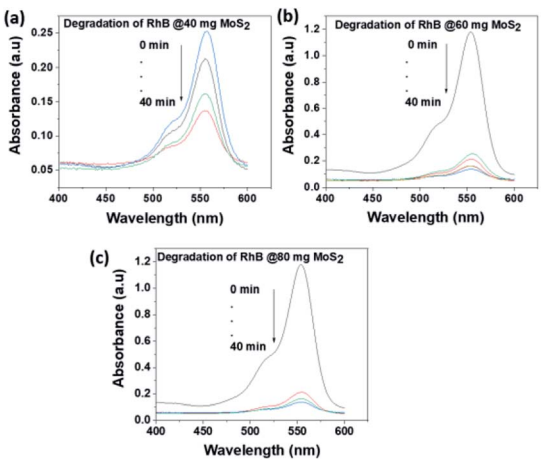

Fig. 12 The effect of MoS_2 NSs dose for the degradation RhB.

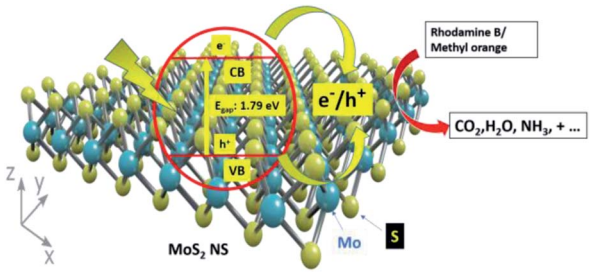

Fig. 13 The plausible degradation mechanism of organic dye.

30 mg). Results showed that fast catalytic activity of MoS_2 NSs observed as a dosage increases from 20 mg to 30 mg. However, yet there is no significant difference between 20 mg and 30 mg dosages, and therefore 20 mg of could be considered as optimum for 50 mL MO (20 mg L^{-1}). The same analogy was observed for RhB degradation. As shown in Fig. 12, the degradation of RhB (50 mL, 20 mg L^{-1}) was investigated at various doses of MoS_2 NSs (40 mg, 60 mg, and 80 mg). The degradation efficiency increases with an increasing dose of MoS_2 NSs. The maximum value was obtained at 80 mg MoS_2 NSs dose, considered as optimum.

3.3. Photocatalytic mechanism

Fig. 13 shows the photocatalytic degradation mechanism of organic dye using catalysts. Firstly, the dye adsorbed on the surface of the MoS_2 NSs in the dark because of the interaction between the shade and MoS_2 NSs. Owing to the low bandgap of the MoS_2 nanosheets, electrons and holes are generated. Electrons in the conduction band react with the available oxygen to form superoxide radicals ($O_2^{\bullet}$). Similarly, holes in the valence band react with water to form hydroxyl ($OH^{\bullet}$) radicals. The formation of the $OH^{\bullet}$ and $O_2^{\bullet}$ radicals has appeared. As a result, the generated OH radicals degrade the adsorbed dyes efficiently at room temperature by simple magnetic stirring. The production of radicals results in the mineralization of dyes into CO_2, H_2O, and other gaseous products.

3.4. Anti-fungal activity of MoS_2 nanosheets

The antimicrobial activity of MoS_2 NSs against standard strains of *Trichophyton mentagrophytes* and *Penicillium chrysogenum* presented in Fig. 14. The higher inhibition zone is observed in *Penicillium chrysogenum* with higher concentrations of the synthesized material, *i.e.*, 5 μg mL^{-1} of MoS_2 nanosheet solutions. Mainly due to the increase in concentrations of MoS_2 nanosheets, the diameter of the inhibition zone increased, *i.e.* 10 mm at 1 μg mL^{-1}, 14 mm at 3 μg mL^{-1} and 16 mm at 5 μg mL^{-1}. At higher concentrations, the diameter of the inhibition zone was more than the same concentrations of the standard drug inhibition (fluconazole (5 μg mL^{-1})). This result shows that a newly prepared nanosheet shows promising and requires further study for antifungal-related applications.

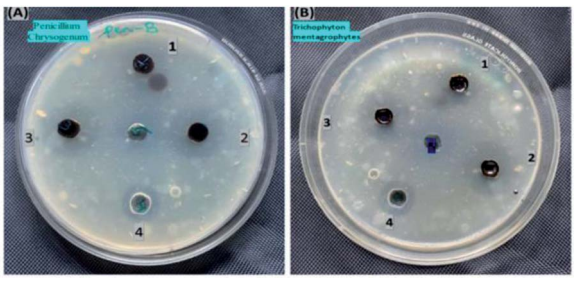

Fig. 14 The antifungal activities of synthesized MoS_2 nanosheet against (A) *Penicillium chrysogenum* and (B) *Trichophyton mentagrophytes*.

4. Conclusions

In conclusion, MoS_2 NSs are synthesised successfully *via* a simple and green hydrothermal method using ammonium molybdenum hydrate and L-cysteine. In this process, to help the growth of MoS_2 NSs, L-cysteine can be used as a sulfur source and a capping agent. The synthesized MoS_2 NSS exhibited excellent photocatalytic degradation efficiency towards MO and RhB dyes under sunlight irradiation. It was achieved >99% degradation efficiency relatively fast rate reaction. The narrow bandgap (1.79 eV), and large surface area (6.46 m^2 g^{-1}) of the MoS_2 NSs are responsible for the degradation of the dyes under sunlight. MoS_2 NSs shows the toxic effect against fungi growth.

Conflicts of interest

There are no conflicts to declare.

Acknowledgements

The authors acknowledge Prof. K. Basavaiah for helpful discussions and giving guides. In addition, my friend Dr Neway Belachew contributes his role to accomplish this work. The authors also acknowledge the Ethiopian Government for financial assistance.

References

1 R. Kant, *Nat. Sci.*, 2012, **4**, 22–26.
2 A. S. M. Raja, A. Arputharaj, S. Saxena and P. G. Patil, *Water in Textiles and Fashion*, 2019, pp. 155–173.
3 N. Belachew, D. Rama Devi and K. Basavaiah, *J. Mol. Liq.*, 2016, **224**, 713–720.
4 V. Katheresan, J. Kansedo and S. Y. Lau, *J. Environ. Chem. Eng.*, 2018, **6**, 4676–4697.
5 N. Belachew, M. H. Kahsay, A. Tadesse and K. Basavaiah, *J. Environ. Chem. Eng.*, 2020, **8**, 104106.
6 D. Chen, Y. Cheng, N. Zhou, P. Chen, Y. Wang, K. Li, S. Huo, P. Cheng, P. Peng, R. Zhang, L. Wang, H. Liu, Y. Liu and R. Ruan, *J. Cleaner Prod.*, 2020, **268**, 121725.
7 M. H. Kahsay, A. Tadesse, D. RamaDevi, N. Belachew and K. Basavaiah, *RSC Adv.*, 2019, **9**, 36967–36981.
8 F. Fresno, R. Portela, S. Suárez and J. M. Coronado, *J. Mater. Chem. A*, 2014, **2**, 2863–2884.

9 A. B. Djurišić, Y. H. Leung and A. M. C. Ng, *Mater. Horiz.*, 2014, **1**, 400.
10 F. Kang, G. Sun, P. Boutinaud, H. Wu, F.-X. Ma, J. Lu, J. Gan, H. Bian, F. Gao and S. Xiao, *Chem. Eng. J.*, 2021, **403**, 126099.
11 A. Wang, F. Kang, Z. Wang, Q. Shao, Z. Li, G. Zhu, J. Lu and Y. Y. Li, *Adv. Sustainable Syst.*, 2019, **3**, 1800132.
12 A. Wang, Y.-L. Hou, F. Kang, F. Lyu, Y. Xiong, W.-C. Chen, C.-S. Lee, Z. Xu, A. L. Rogach, J. Lu and Y. Y. Li, *J. Mater. Chem. C*, 2019, **7**, 2207–2211.
13 Z. Yu, L. Tetard, L. Zhai and J. Thomas, *Energy Environ. Sci.*, 2015, **8**, 702–730.
14 B. Luo, G. Liu and L. Wang, *Nanoscale*, 2016, **8**, 6904–6920.
15 R. Hu, G. Liao, Z. Huang, H. Qiao, H. Liu, Y. Shu, B. Wang and X. Qi, *J. Hazard. Mater.*, 2021, **405**, 124179.
16 J. Kaur, M. Singh, C. Dell'Aversana, R. Benedetti, P. Giardina, M. Rossi, M. Valadan, A. Vergara, A. Cutarelli, A. M. I. Montone, L. Altucci, F. Corrado, A. Nebbioso and C. Altucci, *Sci. Rep.*, 2018, **8**, 16386.
17 M. Singh, C. Zannella, V. Folliero, R. Di Girolamo, F. Bajardi, A. Chianese, L. Altucci, A. Damasco, M. R. Del Sorbo, C. Imperatore, M. Rossi, M. Valadan, M. Varra, A. Vergara, G. Franci, M. Galdiero and C. Altucci, *Front. Bioeng. Biotechnol.*, 2020, **8**, 1056.
18 J. Kaur, A. M. Gravagnuolo, P. Maddalena, C. Altucci, P. Giardina and F. Gesuele, *RSC Adv.*, 2017, **7**, 22400–22408.
19 J. Kaur, A. Vergara, M. Rossi, A. M. Gravagnuolo, M. Valadan, F. Corrado, M. Conte, F. Gesuele, P. Giardina and C. Altucci, *RSC Adv.*, 2017, **7**, 50166–50175.
20 B. Radisavljevic, A. Radenovic, J. Brivio, V. Giacometti and A. Kis, *Nat. Nanotechnol.*, 2011, **6**, 147–150.
21 X. Li and H. Zhu, *J. Materiomics*, 2015, **1**, 33–44.
22 S. Wi, H. Kim, M. Chen, H. Nam, L. J. Guo, E. Meyhofer and X. Liang, *ACS Nano*, 2014, **8**, 5270–5281.
23 K. F. Mak, C. Lee, J. Hone, J. Shan and T. F. Heinz, *Phys. Rev. Lett.*, 2010, **105**, 136805.
24 M. H. Mokari-Manshadi, M. Mahani, Z. Hassani, D. Afzali and E. Esmaeilzadeh, *J. Nanosci. Nanotechnol.*, 2017, **17**, 8864–8868.
25 M. Sabarinathan, S. Harish, J. Archana, M. Navaneethan, H. Ikeda and Y. Hayakawa, *RSC Adv.*, 2017, **7**, 24754–24763.
26 Y.-H. Lee, X.-Q. Zhang, W. Zhang, M.-T. Chang, C.-T. Lin, K.-D. Chang, Y.-C. Yu, J. T.-W. Wang, C.-S. Chang, L.-J. Li and T.-W. Lin, *Adv. Mater.*, 2012, **24**, 2320–2325.
27 K. Sheybani and S. Javadpour, *Int. J. Refract. Met. Hard Mater.*, 2020, **92**, 105277.
28 N. Chaudhary, M. Khanuja, Abid and S. S. Islam, *Sens. Actuators, A*, 2018, **277**, 190–198.
29 T. Oztas, H. S. Sen, E. Durgun and B. Ortaç, *J. Phys. Chem. C*, 2014, **118**, 30120–30126.
30 E. Varrla, C. Backes, K. R. Paton, A. Harvey, Z. Gholamvand, J. McCauley and J. N. Coleman, *Chem. Mater.*, 2015, **27**, 1129–1139.
31 A. M. Gravagnuolo, E. Morales-Narváez, S. Longobardi, E. T. da Silva, P. Giardina and A. Merkoçi, *Adv. Funct. Mater.*, 2015, **25**, 2771–2779.
32 I. Uzcanga, I. Bezverkhyy, P. Afanasiev, C. Scott and M. Vrinat, *Chem. Mater.*, 2005, **17**, 3575–3577.
33 M. Rakibuddin, M. A. Shinde and H. Kim, *Electrochim. Acta*, 2020, **349**, 136403.
34 H. K. Sadhanala, S. Senapati, K. V. Harika, K. K. Nanda and A. Gedanken, *New J. Chem.*, 2018, **42**, 14318–14324.
35 P. Singh, Y.-J. Kim, D. Zhang and D.-C. Yang, *Trends Biotechnol.*, 2016, **34**, 588–599.
36 Y. Guo and J. Li, *Mater. Sci. Eng. C*, 2020, **109**, 110511.
37 N. Belachew, D. S. Meshesha and K. Basavaiah, *RSC Adv.*, 2019, **9**, 39264–39271.
38 S.-K. Park, S.-H. Yu, S. Woo, B. Quan, D.-C. Lee, M. K. Kim, Y.-E. Sung and Y. Piao, *Dalton Trans.*, 2013, **42**, 2399–2405.
39 C. P. Veeramalai, F. Li, Y. Liu, Z. Xu, T. Guo and T. W. Kim, *Appl. Surf. Sci.*, 2016, **389**, 1017–1022.
40 J. Georgin, G. L. Dotto, M. A. Mazutti and E. L. Foletto, *J. Environ. Chem. Eng.*, 2016, **4**, 266–275.
41 P. Sinha, A. Datar, C. Jeong, X. Deng, Y. G. Chung and L.-C. Lin, *J. Phys. Chem. C*, 2019, **123**, 20195–20209.
42 H. F. McMurdie, M. C. Morris, E. H. Evans, B. Paretzkin, W. Wong-NG and C. R. Hubbard, *Powder Diffr.*, 1986, **1**, 40–43.
43 T. S. Sahu and S. Mitra, *Sci. Rep.*, 2015, **5**, 12571.
44 N. Belachew and H. Hinsene, *Appl. Water Sci.*, 2020, **10**, 38.
45 G. A. M. Ali, M. R. Thalji, W. C. Soh, H. Algarni and K. F. Chong, *J. Solid State Electrochem.*, 2020, **24**, 25–34.
46 G. Qingquan, M. Xinfu, X. Yu, T. Wei and Z. Hui, *Colloids Surf., A*, 2017, **530**, 33–37.
47 K. C. Lalithambika, K. Shanmugapriya and S. Sriram, *Appl. Phys. A: Solids Surf.*, 2019, **125**, 817.
48 W. Feng, L. Chen, M. Qin, X. Zhou, Q. Zhang, Y. Miao, K. Qiu, Y. Zhang and C. He, *Sci. Rep.*, 2015, **5**, 17422.
49 J. Kibsgaard, Z. Chen, B. N. Reinecke and T. F. Jaramillo, *Nat. Mater.*, 2012, **11**, 963–969.
50 S. Cui, Z. Wen, X. Huang, J. Chang and J. Chen, *Small*, 2015, **11**, 2305–2313.
51 C. Zhang, Z. Wang, S. Bhoyate, T. Morey, B. Neria, V. Vasiraju, G. Gupta, S. Palchoudhury, P. Kahol, S. Mishra, F. Perez and R. Gupta, *C*, 2017, **3**, 33.
52 L. Ge, C. Han, X. Xiao and L. Guo, *Int. J. Hydrogen Energy*, 2013, **38**, 6960–6969.
53 Y. Huang, Y. Chen, C. Hu, B. Zhang, T. Shen, X. Chen and M. Q. Zhang, *J. Mater. Chem.*, 2012, **22**, 10999.